Observation of Synchrotron Sidebands in a Storage-Ring-Based Seeded Free-Electron Laser

M. Labat,[1,4] M. Hosaka,[2] M. Shimada,[3] N. Yamamoto,[2] M. Katoh,[3] and M. E. Couprie[4,*]

[1]*Centre CEA-Saclay, DSM/IRAMIS/SPAM, 91 191 Gif-sur-Yvette, France*
[2]*Nagoya University, Furo-cho, Chikusa-ku, Nagoya 464-8603, Japan*
[3]*UVSOR, Institute for Molecular Science, Myodaiji, Okazaki 444, Japan*
[4]*Synchrotron SOLEIL, Saint Aubin, BP 34, 91 192 Gif-sur-Yvette, France*

(Received 28 July 2008; published 8 January 2009)

Seeded free-electron lasers (FELs) are among the future fourth-generation light sources in the vacuum ultraviolet and x-ray spectral regions. We analyze the seed temporal coherence preservation in the case of coherent harmonic generation FELs, including spectral narrowing and structure degradation. Indeed, the electron synchrotron motion driven by the seeding laser can cause sideband growth in the FEL spectrum.

DOI: 10.1103/PhysRevLett.102.014801 PACS numbers: 41.60.Cr, 42.25.Kb, 42.65.Ky

Single pass free-electron lasers (FELs) are part of the next-generation light sources delivering short pulses in the vacuum ultraviolet to x-ray range for scientific applications, with improved coherence and intensity compared to the third-generation storage ring synchrotron radiation sources. Investigations on the harmonic generation process in FELs are consequently the subject of sustained interest [1–5], since it offers the possibility of extending the tunability range of the source to short wavelengths, thanks to the harmonic content, while preserving a high degree of coherence. In a FEL, the interaction inside an undulator between a relativistic electron beam and an optical wave at the undulator resonant wavelength leads to an energy modulation of the electronic distribution. This induces longitudinal displacements of the particles, according to the so-called synchrotron motion [6], which result in a density modulation at the resonant wavelength enabling coherent emission. The optical field grows exponentially along the undulator to the detriment of the electrons' kinetic energy. Saturation is reached when the electrons become off resonance. In the saturated regime, because the particles keep rotating in the ponderomotive force of the optical field, sidebands can appear in the radiation spectrum and spoil the temporal coherence, as observed in the case of oscillator FELs [7] and of SASE (self-amplified spontaneous emission) FELs [8,9]. In the SASE [10,11] configuration, since the amplified optical wave consists of the electron beam spontaneous emission, the microbunches are uncorrelated, and the SASE FEL exhibits weak temporal coherence [12] with a chaotic temporal structure and a spiky spectrum [13]. In the seeded FEL configuration [3,5], an external laser source provides the initial optical wave and initiates the modulation of the electronic distribution. In addition to a reduction of the saturation length [14], this scheme allows the correlation of the microbunches which leads to a high temporal coherence associated with a single line spectrum [5]. Among seeded FEL configurations, the coherent harmonic generation (CHG) [1,3] enables the enhancement of the harmonic content. An external laser source is injected inside a first undulator—the modulator—where the energy modulation of the electron beam is performed. The conversion into a density modulation occurs in a dispersive section, and the coherent emission with strong harmonic content is produced in a second undulator—the radiator. Thanks to the seeding laser-electron beam interaction in the modulator, CHG FELs finally inherit the coherence properties of the seeding laser and are expected to reproduce their spectral structure [15]. In this Letter, we report an experimental spectral analysis of a CHG FEL as a function of the seeding laser parameters. We show that this laser-electron interaction has to be finely adjusted to prevent the spectral structure from being spoiled by the growth of sidebands as in the oscillator and SASE FEL cases. Relating the evolution of the spectrum to the synchrotron motion in the seeding laser field using PERSEO [16] simulations, we provide key insights on the control of seeded FEL temporal coherence properties.

The experiment was performed on the UVSOR-II storage ring CHG FEL [17,18] (see Fig. 1). The modulator, the dispersive section, and the radiator are the elements of a

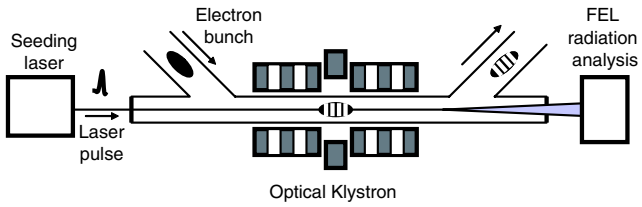

FIG. 1 (color online). Schematic of a CHG FEL. For the UVSOR-II FEL, the electron beam is stored in a single bunch mode at $E = 600$ MeV. Optical klystron: 2 undulators of $N = 9$ periods of 11 cm and a dispersive section of $N_d = 90$ equivalent periods. The seeding laser is at 800 nm, with up to 2 W of average power and a pulse duration ΔT_L of 150–1200 fs-FWHM. The radiation is transported through bandpass filters (P10405A-H972 from Corion for H2, CVI-F25-265.0-3-1.00 from CVI for H3) to a spectrometer (PMA10, Hamamatsu) whose detector is a fast gated intensified CCD camera (C3077-C4078, Hamamatsu).

single structure called an optical klystron (OK) [19]. The seeding laser is focused in the middle of the modulator either with a *strong* focusing corresponding to a Rayleigh length of $Z_R = 0.15$ m (estimated waist at focusing point $w_0 = 200$ μm) or with a *smooth* focusing corresponding to a Rayleigh length of $Z_R = 1.5$ m ($w_0 = 600$ μm). For spectral analysis, the OK radiation is transported to a spectrometer coupled to a fast intensified CCD camera (see Fig. 1). The ultrashort exposure time (down to 2 ns) of this system isolates the spectra of coherent light pulses at the seeding laser's 1 kHz repetition rate from the 5.6 MHz incoherent light pulses.

Typical examples of the CHG FEL and the spontaneous emission (SE) spectra are presented in Figs. 2(a) and 2(b). Because the OK radiation results from the interference between the emission of each undulator, the spontaneous emission spectrum consists of a series of fringes [20]. The overall envelope is centered at the so-called resonant wavelength λ_R:

$$\lambda_R = \frac{\lambda_0}{2\gamma^2}(1 + K^2/2). \quad (1)$$

λ_0 is the undulator period, and $K = 0.0934 \times B_0[\mathrm{T}]\lambda_0[\mathrm{mm}]$ is the deflection parameter of the (planar) undulators, with B_0 the peak magnetic field. λ_R is tuned via the variation of K which depends on the undulator gap g. For an ideal electron beam, the bandwidth is $\frac{1}{nN}$ for the spectrum envelop and $\frac{1}{n(N+N_d)}$ for one single fringe [20]. N and N_d are the number of undulator and dispersive section periods, respectively, while n is the harmonic number. When the seeding laser is injected, additional spectral lines appear around 412 nm [see Fig. 2(a)] and around 266 nm [see Fig. 2(b)]. Those lines correspond to the second and third harmonics of the density modulation wavelength, i.e., of the seeding laser wavelength (400 and 266.6 nm). The

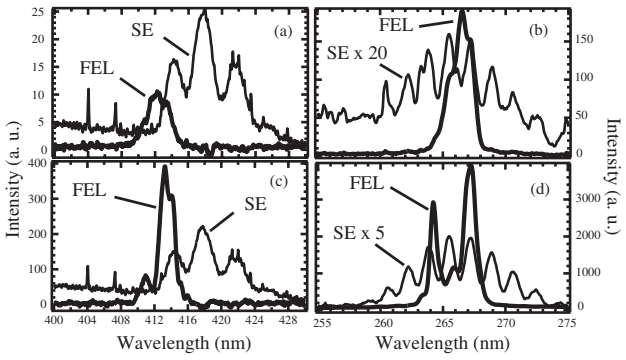

FIG. 2. CHG FEL spectra on the (a) second and (b) third harmonics with the smooth focusing configuration and on the (c) second harmonic (sideband at 410.9 nm) and (d) third harmonics (sidebands at 264.2 and 267.2 nm) with the strong focusing configuration. $g = 40.8$ mm (40.5 mm) for the second (third) harmonic. $P_L = 2$ W, $\Delta T_L = 1$ ps-FWHM. Single shot acquisition. SE spectrum recorded with the laser off and the FEL spectrum with the laser on.

experimental wavelength shift of the second harmonics is due to the collection of off-axis radiation at a longer wavelength [21]. The measured spectral width is $\Delta\lambda = 3$ nm ($\Delta\lambda = 1$ nm) on the second (third) coherent harmonic, while the spontaneous emission spectral width reaches 10 nm on both harmonics. The laser-induced energy modulation results in coherent emission with monochromatic and narrow band spectra on the harmonics of the fundamental. The Fourier product $c\Delta T\frac{\Delta\lambda}{\lambda^2}$, assuming that the pulse duration ΔT of the coherent harmonics equals the duration of the seeding laser pulse, is improved by a factor 70 (2000) on the second (third) harmonic. It becomes only 10 times above the Fourier limit (assuming Gaussian pulses). In addition, unlike the FEL oscillator, for which lasing occurs at the maximum of the spontaneous emission derivative and therefore strongly depends on the undulator gap, the variation of the undulator gap does not modify the coherent emission wavelengths. The CHG FEL wavelengths, corresponding to the harmonics of the electronic distribution modulation period, are set by the seeding laser wavelength. The tunability of the CHG FEL relies on the tunability of the seeding laser. In addition, the operation of the CHG FEL in specific conditions can modify this basic spectral structure: Additional spectral lines appear on each side of the initial line. In the example presented in Figs. 2(c) and 2(d), when using a strong focusing, one sideband appears in the blue part of the second harmonic spectrum at 410.9 nm and two sidebands (in the *red* part at 267.2 nm and in the *blue* part at 264.2 nm) grow in the case of the third harmonic. The undulator gap has again no influence on the position of the sidebands. Nevertheless, the limited undulator bandwidth acts on the coherent radiation as a bandpass filter, centered on the resonant wavelength by gap adjustment, which can eventually cut off a part of the coherent spectrum, i.e., one of the sidebands. The measured amplification bandpass is around 9 nm on the third harmonic, corresponding to a relative bandpass of $3.8(\pm 0.2) \times 10^{-2}$, in good agreement with the expected theoretical value 3.7×10^{-2}. Indeed, in the case of the third harmonic, the FEL emits only on the red sideband for gaps below 40.3 mm. For increasing gap values, the intensity of the blue sideband grows to the detriment of the red sideband, until the red line vanishes around a 40.8 mm gap. Above 41 mm, the FEL emits only on the blue line. In the case of the second harmonic, the two sidebands cannot be observed simultaneously (at the same gap value). Around 40.8 mm, the red sideband appears, while the blue sideband disappears. Such an effect results from the intrinsic FEL process. The FEL pulse amplification requires spectral matching between the modulation and the resonant wavelength [18].

The growth of sidebands in the spectrum is a consequence of the synchrotron motion of the particles [6]. The ponderomotive force of the intense laser electric field drives oscillations of the electrons in the phase space (see Fig. 3) at the synchrotron frequency ω_S [22–24]:

$$\omega_S = \frac{8\pi}{\lambda_0}\sqrt{\frac{e[J_0(\xi) - J_1(\xi)]KE_L}{mk_L(1 + K^2/2)}}, \qquad \xi = \frac{K^2}{4 + 2K^2}. \tag{2}$$

J_q is the Bessel function of order q, $k_L = \frac{2\pi}{\lambda_L}$, with λ_L the laser wavelength, m is the mass, and e is the charge of the electron. This synchrotron motion leads to a density modulation of the electronic distribution in phase space (see Fig. 3) and enables coherent emission. The synchrotron frequency depends on the undulator magnetic field via the deflection parameter K and on the laser optical field amplitude E_L:

$$|E_L|^2 = \sqrt{2}P_L[c\epsilon_0\pi f_{\mathrm{rep}}\lambda_L Z_R\sigma_L]^{-1} \tag{3}$$

via the average power P_L, the rms pulse duration σ_L, and the Rayleigh length Z_R. The seeding laser parameters provide a main control on the synchrotron frequency, i.e., of the particle motion velocity. As illustrated in Fig. 3, for an increasing seeding laser power, the particles experience a larger displacement in phase space, getting deeper in their rotation cycle. For 0.5 W seeding power, the bunching (density modulation) is optimum, and the associated third harmonic spectrum is monochromatic. For 1 W seeding power, the debunching (spoiling of the density modulation) starts while sidebands appear in the associated spectrum. Higher seeding power drives faster dynamics of the particles, resulting in the fast growth of the sidebands to the detriment of the initial central line. For 2 W seeding power, the central line has nearly vanished while a second pair of sidebands appears. The movement of the particles modulates the FEL radiation electric field at ω_S in the electronic frame, which results in a modulation at frequency $\Omega_{\mathrm{SB}} = \frac{2\gamma^2}{(1+K^2/2)}\omega_S$ in the laboratory frame. The FEL field now consists of three frequency components at ω_L and $\omega_L \pm \Omega_{\mathrm{SB}}$. In the spectral domain, this additional content corresponds to a pair of sidebands shifted by $\Delta\lambda_{\mathrm{SB}} = \pm\frac{\lambda^2}{2\pi c}\Omega_{\mathrm{SB}}$ with respect to the initial central line (see Fig. 3). The modulation is strongly enhanced when the particles perform an integer number p of cycle(s) in phase space while the radiation passes through the optical klystron, i.e., when the synchrotron period in the laboratory frame is a harmonic of the time required for the radiation to pass through the undulator: $(2N + N_d)\lambda_L/c$. Back in the electronic frame, the modulation amplification is then expected for $\omega_S \geq \frac{2\pi c}{(2N+N_d)\lambda_0}$, driving sidebands shifted by 1.8 nm on the second and 0.9 nm on the third harmonic. The threshold is $\omega_S \geq 1.6 \times 10^8$ Hz, while in the standard conditions of operation ($P_L = 2$ W, $\Delta T_L = 1.2$ ps-FWHM, and $Z_R = 0.15$ m) $\omega_S = 2.7 \times 10^8$ Hz. In agreement with the predictions, sidebands resulting from a modulation amplification are observed, respectively, with 3.5 and 2 nm shifts on the second and third harmonics. A strong field drives a fast motion of the particles which in turn modulates the optical field. This effect is enhanced when the modulation frequency couples to the interaction frequency, leading to the growth of sidebands. The analytical considerations are in good qualitative and quantitative agreement with the experimental results. The PERSEO simulations reproduce the sideband growth in the case of an overbunched beam by a strong seeding optical field [Fig. 3(b), (i)–(iv)] and the further disappearance of the central line [Fig. 3(b), (v)].

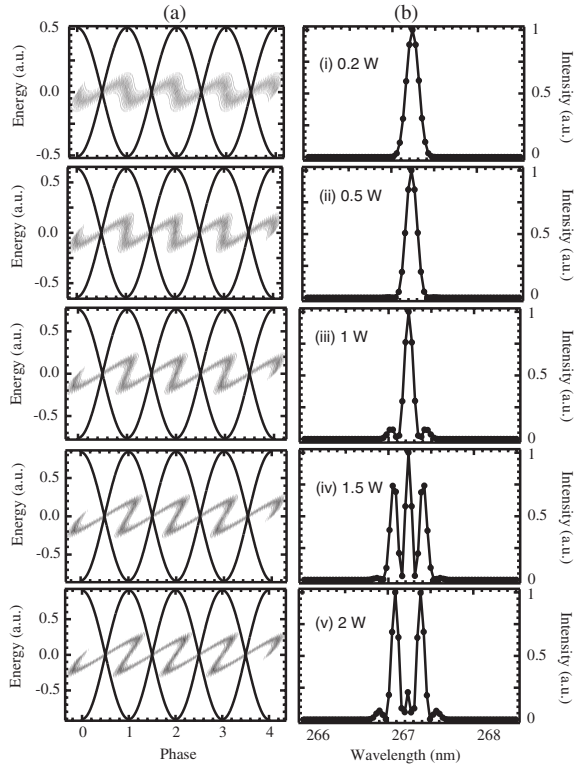

FIG. 3. (a) Evolution of the center of the electronic distribution in the phase space and (b) of the FEL radiation spectrum on the third harmonic at the optical klystron output as a function of the seeding power. (a) Solid line for the laser electric field, dotted line for the electrons. Simulation with PERSEO: $E = 600$ MeV, $\sigma_\gamma = 3.4 \times 10^{-4}$, $\epsilon_{x,y} = 3\pi$ mm mrad, $\beta = 6$ m, $\Delta T_L = 1$ ps-FWHM, $K = 6.18$, $N_d = 100$, and $\lambda_R = \lambda_L = 801.7$ nm.

The FEL third harmonic spectral lines measured as a function of the laser parameters are presented in Fig. 4. With the maximum available pulse duration, a strong focusing, and a low seeding power, the FEL radiation consists of a single spectral line (●). With increasing seeding average power, sidebands appear around 1 W (□), which gives an experimental threshold for sideband growth around 0.8 W on the seeding power. The calculation of the expected power threshold using Eqs. (2) and (3) leads to 0.25 W, in reasonable agreement with measurements considering that the energy transfer is reduced by the size mismatch of the beams, i.e., reduced transverse overlap, by more than 50%. A power increase from 1 to 2 W did not cause a significative shift of the sideband positions. The calculated variation corresponds to an additional spectral shift of 0.2 nm, which is below the spectrometer resolution. The influence of the laser Rayleigh length on the FEL

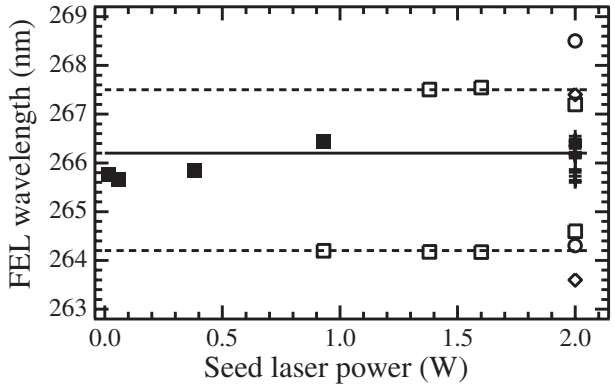

FIG. 4. Third coherent harmonic wavelengths vs power. Solid markers and (+): Central line; empty markers: sidebands. $\Delta T_L =$ 1.0 ps-FWHM: (■) and (□) with strong focusing and $g =$ 40.5 mm, (+) with smooth focusing and gap ranging from 39.8 to 41.7 mm. (◇) $\Delta T_L = 0.5$ ps-FWHM and (○) $\Delta T_L =$ 0.25 ps-FWHM with strong focusing and $g = 40.5$ mm.

spectrum is also illustrated in Fig. 4. Using a smooth focusing (long Rayleigh length) with a long pulse duration, the spectrum is monochromatic (+) whatever the peak power. The maximum ω_S (1.5×10^8 Hz) remains below the calculated threshold (1.6×10^8 Hz): The motion is not fast enough for the particles to perform within one pass a complete cycle in the phase space and consequently generate sidebands in the spectrum. Using a strong focusing, additional spectral lines are observed [see (□) and (△) in Fig. 4], as expected since the synchrotron frequency overpasses the threshold (ω_S reaches 2.7×10^8 Hz). The introduction of a chirp in the laser pulse increases the seeding laser pulse duration. Nevertheless, as expected from Eqs. (2) and (3), with a strong focusing and maximum seeding power, the maximum ΔT_L available does not allow the sidebands to be suppressed since the synchrotron frequency is already above the threshold (2.7×10^8 Hz). Still, the reduction of the pulse duration, corresponding to a synchrotron frequency increase, now enables one to detect a shift of the sideband positions [see (△), (▲), and (○) in Fig. 4]. The distance between the sideband lines increases by 1.2 nm when reducing the pulse duration by a factor of 4, in agreement with the 1.4 nm expected from $\Delta\lambda_{\mathrm{SB}} = \pm\frac{\lambda^2}{2\pi c}\Delta\Omega_{\mathrm{SB}}$. The pulse duration decrease also causes a displacement of the sideband lines towards the long wavelengths (by 0.5 nm when reducing the pulse duration from 1.2 to 0.25 ps-FWHM). From the derivative of Eq. (1), $\frac{\partial\gamma}{\gamma} = -\frac{\partial\lambda}{2\lambda}$: The optical power increase via pulse duration decrease causes an additional energy loss $\partial\gamma$ of the particles which shifts the radiation spectrum by $\partial\lambda$ to the red. The same effect can be noticed on the second harmonic when moving from smooth to strong focusing (0.8 nm spectral shift) and on the third harmonic when increasing the seeding power (less than 0.5 nm from 0 to 0.9 W; see Fig. 4). The FEL spectral structure is highly sensitive to Z_R, ΔT_L, and P_L.

In conclusion, we have presented an analysis of a CHG FEL spectral structure. We show that the seeding laser parameters drive the electron synchrotron motion which itself determines the final FEL spectrum. The experimental measurements are in agreement with both PERSEO simulations and analytical considerations. Finally, the use of an external laser source allows the generation of coherent pulses together with a fine control of the output spectral structure. This gives an interesting insight into the optimization of the coherence properties of any seeded FEL configuration, including next-generation seeded x-ray FELs.

*marie.labat@enea.it

[1] R. Coisson and F. De Martini, *Physics of Quantum Electronics* (Addison-Wesley, Reading, MA, 1982), Vol. 9, p. 939.
[2] R. Bonifacio *et al.*, Nucl. Instrum. Methods Phys. Res., Sect. A **293**, 627 (1990).
[3] L. H. Yu *et al.*, Phys. Rev. A **44**, 5178 (1991).
[4] Z. Huang and K. J. Kim, Phys. Rev. E **62**, 7295 (2000).
[5] L. H. Yu *et al.*, Science **289**, 932 (2000).
[6] W. Colson and A. Renieri, J. Phys. (Paris) **44**, C1 (1983).
[7] R. W. Warren *et al.*, Nucl. Instrum. Methods Phys. Res., Sect. A **285**, 1 (1989).
[8] A. H. Lumpkin *et al.*, Phys. Rev. Lett. **88**, 234801 (2002).
[9] V. Sajaev *et al.*, Nucl. Instrum. Methods Phys. Res., Sect. A **506**, 304 (2003).
[10] A. M. Kondratenko and E. L. Saldin, Sov. Phys. Dokl. **24**, 986 (1979).
[11] B. Bonifacio *et al.*, Opt. Commun. **50**, 373 (1984).
[12] R. Bonifacio *et al.*, Phys. Rev. Lett. **73**, 70 (1994).
[13] E. Saldin *et al.*, Opt. Commun. **148**, 383 (1998).
[14] L. H. Yu *et al.*, Phys. Rev. Lett. **91**, 074801 (2003).
[15] A. Doyuran *et al.*, Phys. Rev. ST Accel. Beams **7**, 050701 (2004).
[16] L. Giannessi, in *Proceedings of the FEL'06 Conference, Berlin, Germany* (http://www.jacow.org/, 2006), Vol. 1, pp. 91–94.
[17] M. Hosaka *et al.*, Nucl. Instrum. Methods Phys. Res., Sect. A **528**, 291 (2004).
[18] M. Labat *et al.*, Eur. Phys. J. D **44**, 187 (2007).
[19] N. A. Vinokurov and A. N. Skrinsky, Nuclear Physics Institute of Novosibirsk, Report No. 77-59, 1977.
[20] P. Elleaume, J. Phys. (Paris) **44**, C1 (1983).
[21] H. Onuki and P. Elleaume, Taylor & Francis, London, 2003.
[22] N. M. Kroll *et al.*, IEEE J. Quantum Electron. **17**, 1436 (1981).
[23] L. Giannessi *et al.*, *Proceedings of the FEL'05 Conference, Stanford, CA* (http://www.jacow.org/, 2005), Vol. 1, p. 210.
[24] This synchrotron frequency characterizes the particle motion in the laser electric field, while the accelerator synchrotron frequency [25] used in the storage ring community refers to the particle motion in the rf cavity electric field and ranges in another frequency domain (≈kHz).
[25] M. Sands, SLAC Report No. 121, 1970.